Wind and Structures, Vol. 7, No. 6 (2004) 359-372
DOI: http://dx.doi.org/10.12989/was.2004.7.6.359

Fluctuating wind loads across gable-end buildings with planar and curved roofs

J. D. Ginger†

Cyclone Testing Station, School of Engineering, James Cook University, Townsville, Qld 4811, Australia
(Received July 11, 2003, Accepted August 2, 2004)

Abstract. Wind tunnel model studies were carried out to determine the wind load distribution on tributary areas near the gable-end of large, low-rise buildings with high pitch planar and curved roof shapes. Background pressure fluctuations on each tributary area are described by a series of uncorrelated modes given by the eigenvectors of the force covariance matrix. Analysis of eigenvalues shows that the dominant first mode contributes around 40% to the fluctuating pressures, and the eigenvector mode-shape generally follows the mean pressure distribution. The first mode contributes significantly to the fluctuating load effect, when its influence line is similar to the mode-shape. For such cases, the effective static pressure distribution closely follows the mean pressure distribution on the tributary area, and the quasi-static method would provide a good estimate of peak load effects.

Keywords: gable-end building; roof shape; wind load; influence coefficient; wind load effect; eigenvector; eigenvalue; effective static pressure.

1. Introduction

Large, gable-end buildings with high pitch planar or curved roofs are used in many industrial applications. The structural system of such buildings typically consists of portal or pin-jointed frames (or trusses), spaced evenly in the inner part and sometimes closer together near the gable-ends. Metal sheet cladding is attached to roof purlins and wall girts, which are fixed to these frames. Wind loading is an important structural design load consideration.

Spatially and temporally varying pressures on the tributary area generates fluctuating wind load effects (i.e., bending moments, shear forces etc.) on the structural system. These wind load effects can be resolved in terms of a mean component averaged over time and a fluctuating part, comprising of resonant response resulting from excitation at the natural frequencies of the structure and background response produced by fluctuations at other frequencies. For most low-rise buildings, the wind loading frequencies are much lower than the natural frequency of the structure, and the resonant response is negligible. Wind loading standards such as AS/NZS 1170.2 (2002) and ASCE 7 (2002) use the quasi-static method for deriving design wind loads on these "static" structures, where the background response is assumed to follow the mean loading pattern. However, the effective pressure distributions producing some peak load effects can have a different pattern to the mean loads, and the quasi-static approach can provide unsatisfactory design load effects. The main

† Senior Lecturer

factors determining these effective pressure distributions are the influence line for the particular load effect and the correlation of the wind pressures acting on the tributary area.

The “covariance integration” method developed by Holmes and Best (1981) can be used to calculate wind load effects of interest to the structural designer. Holmes (1988) extended this method, by representing the background pressure fluctuations over the tributary area by a series of eigenvector mode-shapes weighted by the corresponding eigenvalues. Kasperski and Niemann (1989) developed the “load-response-correlation” method (LRC), which gives the effective static pressure distribution on the tributary area. Holmes (1992, 2002) further refined these methods and summarized their applications in wind engineering.

The pressure distributions across tributary areas near the gable-end of large, low-rise industrial buildings with high pitch planar and curved roof shapes are studied in this paper. The correlation of pressures on these tributary areas are analysed to determine the dominant eigenvector mode-shapes and corresponding eigenvalues - a measure of the contribution from each mode to the total pressure fluctuations. The relationship between mode-shapes of pressure fluctuations, the influence line for a particular load effect and corresponding effective static pressure distributions are studied.

2. Wind flow over gable-end buildings

Wind flow and resulting pressure characteristics on a building are mainly influenced by its roof shape and pitch, length to span aspect ratio and height. The roof shape and pitch are generally dictated by functional requirements and structural efficiency. For example, high pitch planar and arched roofs are used in structures such as aircraft hangars, ship dry-docks and bulk material storage facilities.

Wind blowing normal to the ridge of a high roof pitch ($>30^{o}$) building causes flow separation to take place along the ridge-line forming a large vortex on the leeward roof and wall. In the case of a steeply curved or arched roof, separation usually occurs downstream from the apex. For oblique approach winds, flow separation takes place along the windward roof edges at the gable-end and eave, and also the ridge-line in the case of high pitch roofs, forming a series of conical vortices. The suction pressures under these conical vortices are extremely large, especially at their apex, near the windward gable-end, eave and ridge corners. Critical design (i.e., peak) wind load effects on the structural system near the gable-end of these large buildings are frequently measured for oblique approach winds (Ginger and Holmes 2001).

For approach wind parallel to the ridge of a planar roof, or the axis of a curved roof, flow separation takes place at the windward roof edge at the gable-end, forming a “separation bubble” with a mean reattachment length of about 2.5 times the average roof height. The pressure distributions have similar characteristics irrespective of roof pitch and shape.

3. Wind loads and effective pressure distributions

The pressure at i, $p_i(t)$ is described in terms of the mean pressure averaged over time t $\overline{p}_i$, and the fluctuating component $p'_i(t)$ as shown in Eq. (1). Maximum and minimum (i.e., peak) pressures $\hat{p}_i$ and $\breve{p}_i$ are given by Eq. (2), where g_{p_i} is the pressure peak factor and σ_{p_i} is the standard deviation.

$$p_i(t) = \overline{p}_i + p'_i(t) \tag{1}$$

$$\hat{p}_i, \breve{p} = \overline{p}_i \pm g_{p_i}\, \sigma_{p_i} \tag{2}$$

The load effect $x(t)$ resulting from wind loading on a tributary area consisting of N panels is given by Eq. (3), where β_i and P_i are the influence coefficient and load at panel i of area A_i, and $\overline{x}$ and x' are the mean and fluctuating parts of x.

$$x(t) = \sum_{i=1}^{N} \beta_i p_i(t) A_i = \sum_{i=1}^{N} \beta_i P_i(t) = \sum_{i=1}^{N} \beta_i (\overline{P}_i + P'_i(t)) = \overline{x} + x'(t) \tag{3}$$

Holmes and Best (1981) developed the covariance integration method given in Eqs. (4) and (5) to obtain the peak value of a load effect, $\hat{x}$ (or $\breve{x}$), where σ_x is the standard deviation and g_x is the peak factor of x.

$$\hat{x}, \breve{x} = \overline{x} \pm g_x \sigma_x \tag{4}$$

$$\sigma_x = \left[\sum_{i=1}^{N} \sum_{j=1}^{N} \beta_i \beta_j \overline{P'_i(t) P'_j(t)} \right]^{1/2} = \left[\sum_{i=1}^{N} \sum_{j=1}^{N} \beta_i \beta_j r_{p_i p_j} \sigma_{p_i} \sigma_{p_j} A_i A_j \right]^{1/2} \tag{5}$$

Here, $r_{p_i p_j} = \overline{p'_i(t) p'_j(t)} / (\sigma_{p_i} \sigma_{p_j})$ is the correlation coefficient between pressures at i and j, and the peak factor, g_x is calculated as described by Ginger and Holmes (2003).

3.1. Eigenvalue representation

The spatial and temporal variation of wind loads on a tributary area can be represented by a series of orthonormal modes. Holmes (1988) showed that the force covariance matrix $\overline{P'_i(t) P'_j(t)}$ for $i, j = 1..N$, can be analyzed in proper orthogonal decomposition form shown in Eq. (6), where e_{in} is the eigenvector component at position i and $\overline{a_n^2(t)} = \lambda_n$ is the eigenvalue for the *nth* mode.

$$P'_i(t) = \sum_{n=1}^{N} e_{in} a_n(t), \qquad P'_j(t) = \sum_{k=1}^{N} e_{jk} a_k(t) \tag{6}$$

Applying eigenvector expansions from Eq. (6) to Eq. (5) gives,

$$\sigma_x^2 = \sum_{i=1}^{N} \sum_{j=1}^{N} \left[\overline{\sum_{n=1}^{N} e_{in} a_n(t) \sum_{k=1}^{N} e_{jk} a_k(t)} \right] \beta_i \beta_j \tag{7}$$

According to Holmes (1992), defining $\alpha_n = \sum_{i=1}^{N} e_{in} \beta_i$, and noting that $\overline{a_n(t) a_k(t)} = 0$, for $n \neq k$, gives;

$$\sigma_x^2 = \sum_{n=1}^{N} \alpha_n^2 \lambda_n \tag{8}$$

Each eigenvector mode describes a distinct loading mechanism, and the eigenvalue represents the contribution by the mode to the total load fluctuations. Previous studies have shown that the first few modes contribute the most to the fluctuating wind load. Eq. (8) indicates that the variance of a load effect is derived from summing the combination of the square of influence coefficient and eigenvector, with the eigenvalue of each mode. The effectiveness of the quasi-static method for deriving peak load effects can be assessed by comparing the dominant mode-shapes with the mean pressure distribution on the tributary area, and calculating the percentage contributions from each mode to the fluctuating load effect.

3.2. Equivalent static pressure distribution

Kasperski and Niemann (1989) derived Eq. (9) for the load at j, P_j which generates the peak value of load effect $\hat{x}$ (or $\breve{x}$). The "load response correlation" (LRC) method given by Eqs. (9) and (10) is used to determine the equivalent static load distribution for the selected load effect.

$$(P_j)_{\hat{x},\breve{x}} = \overline{P_j} \pm g_x r_{P_j x} \sigma_{P_j} \tag{9}$$

Here, $r_{P_j x}$ is the correlation coefficient between the wind load fluctuations at j and the load effect x. Following Holmes (1992) and noting that $\overline{a_n(t)a_k(t)} = 0$ for $n \neq k$, and $\overline{a_n^2(t)} = \lambda_n$, gives

$$r_{P_j x}\sigma_{P_j} = \left[\sum_{n=1}^{N} \alpha_n e_{jn} \lambda_n\right] \Big/ \left[\sum_{n=1}^{N} \alpha_n^2 \lambda_n\right]^{1/2} \tag{10}$$

Eq. (10) shows that the fluctuating component of the effective static pressure at panel j is composed of the product of eigenvector for each mode and influence coefficient of the selected load effect combined with the eigenvector component and eigenvalue.

4. Wind tunnel tests

Wind tunnel model tests were carried out in the 2.0 m high $\times$ 2.5 m wide $\times$ 22 m long Boundary Layer Wind Tunnel at the Cyclone Testing Station, School of Engineering, James Cook University, in Townsville, Australia. Two building configurations described in Table 1, and shown in Fig. 1 were tested at a length scale of 1/200 in simulated open (i.e., terrain category 2 as per AS/NZS 1170.2 (2002), exposure C as per ASCE 7 (2002)) approach atmospheric boundary layer flows. The curved roof surface of building configuration 2 was roughened such that the air-flow over the surface was representative of higher Reynolds Number full-scale conditions. Area-averaged external pressures were measured for θ at 15^{o} intervals, on wall and roof panels 1..10 and 1..9, of tributary

Table 1 Test building configurations and specifications

Configuration	Roof Pitch (^{o})	Span (d), m	Mid-roof height, m	Total height, m	Eaves height, m	Length, m	Frame height (h_f), m
1	35	40	22	29	15	160	21.5
2	Curved	30	15	20	10	120	20

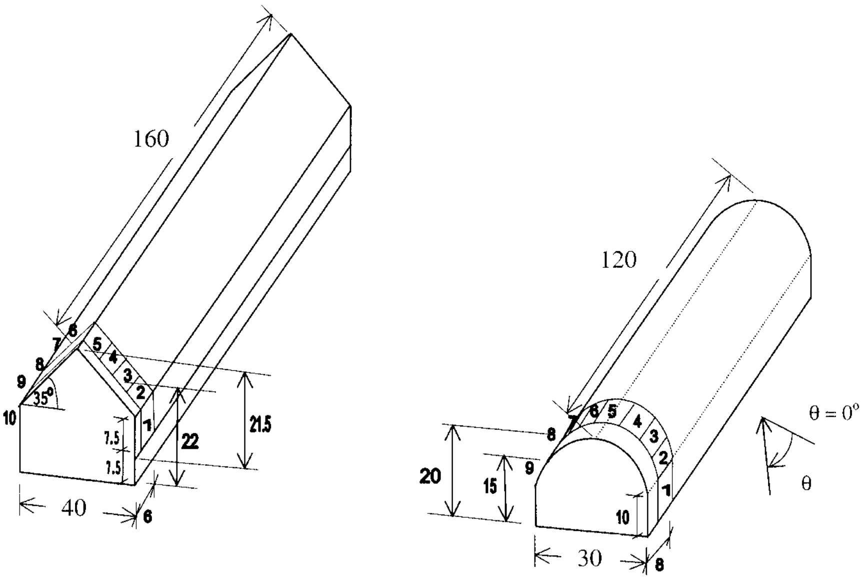

Fig. 1 Building configurations 1 and 2 showing frame tributaries and panels near gable-end all dimensions in m, not to scale

areas on building configurations 1 and 2 respectively, shown in Fig. 1. Tuned, manifold-tube-restrictor systems connected to pressure transducers via Scanivalves were used to measure these fluctuating pressures which were low-pass filtered at a frequency of 250 Hz, and sampled at 500 Hz for 24 secs for a single run. The pressures were analyzed and recorded as mean, standard deviation, maximum and minimum pressure coefficients;

$$C_{\overline{p}} = \overline{p} / \left(\frac{1}{2}\rho \overline{U}_h^2\right), \quad C_{\sigma_p} = \sigma_p / \left(\frac{1}{2}\rho \overline{U}_h^2\right), \quad C_{\hat{p}} = \hat{p} / \left(\frac{1}{2}\rho \overline{U}_h^2\right) \text{and } C_{\breve{p}} = \breve{p} / \left(\frac{1}{2}\rho \overline{U}_h^2\right)$$

where, $\frac{1}{2}\rho \overline{U}_h^2$ is the mean dynamic pressure at the reference, mid-roof height h.

The results were derived from averaging the pressure coefficients obtained from five runs. The external pressure acting towards the surface is defined positive. The correlation coefficients between pressures acting on panels on these tributary areas were also measured.

5. Pressure distributions

Wind load effects for structural design of low-rise buildings are usually calculated from equivalent static pressures derived from the nominal shape factors or pressure coefficients, provided in standards such as AS/NZS 1170.2 (2002) and ASCE 7 (2002). Results from these wind tunnel tests showed that design values for load effects of interest studied here were measured for oblique winds approaching at $\theta = 45^{\circ}$. The wind approach direction $\theta = 0^{\circ}$ in AS/NZS 1170.2 (2002) and ASCE 7 (2002) covers this design condition. The distribution of mean, standard deviation, maximum and

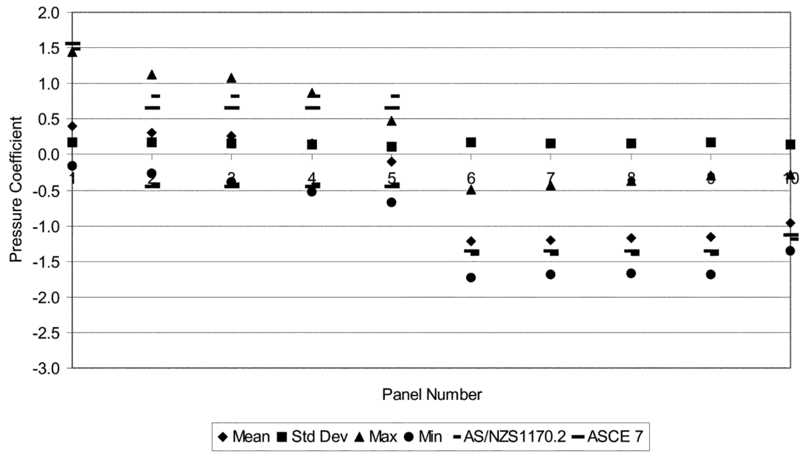

Fig. 2 Mean, standard deviation, maximum and minimum pressure coefficients on building configuration 1, $\theta = 45^{o}$ and effective peak pressure coefficients from AS/NZS 1170.2 and ASCE 7, $\theta = 0^{o}$

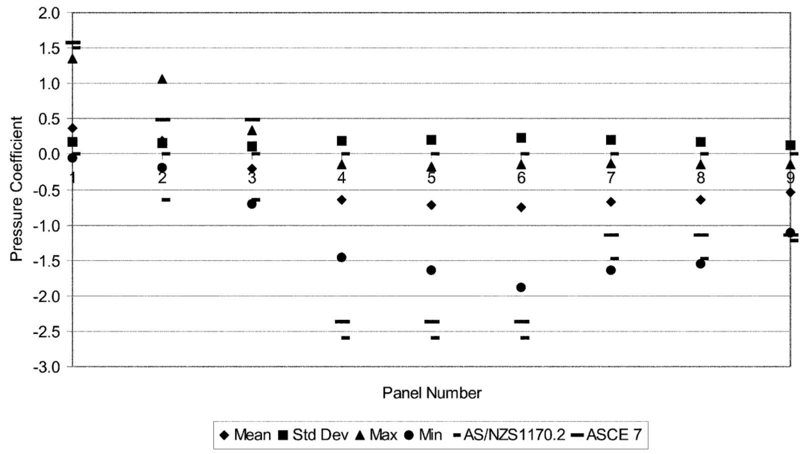

Fig. 3 Mean, standard deviation, maximum and minimum pressure coefficients on building configuration 2, $\theta = 45^{o}$ and effective peak pressure coefficients from AS/NZS 1170.2 and ASCE 7, $\theta = 0^{o}$

minimum, area-averaged panel pressure coefficients, for $\theta = 45^{o}$ on building configurations 1 and 2, and for $\theta = 90^{o}$ on building configuration 1 and 2 are given in Figs. 2, 3, 4 and 5 respectively. Effective peak pressure coefficients calculated from AS/NZS 1170.2 (2002) as $C_{peak} = C_{fig} \times G_U^2 = (C_{p,e} \times K_a \times K_c \times K_l \times K_p) \times G_U^2$, and from ASCE 7 (2002) as, $C_{peak} = GC_p \times G_U^2 = (0.85C_p) \times G_U^2$, are also presented in Figs. 2 to 5. The quasi-static external pressure coefficients, $C_{p,e}$ and C_p for the planar and curved roofs are obtained from Clause 5.4 of Section 5, and Clause C3 of Appendix C in AS/NZS 1170.2, and Fig. 6.6 and Table 6.8 in ASCE 7 respectively. Here, K_a, K_c, K_l and K_p are factors for area-averaging, load combination, local-pressure effects, and cladding permeability, where, $K_l = 1.0$, because the analysis is carried out on primary structural components, $K_p = 1.0$, as the cladding is non-porous, and $K_a \times K_c = 0.8$, for wind loads acting on a tributary area larger than 100 m^2. The velocity gust factor G_U is taken as 1.628 and 1.640, at the mid-roof heights of 22 m

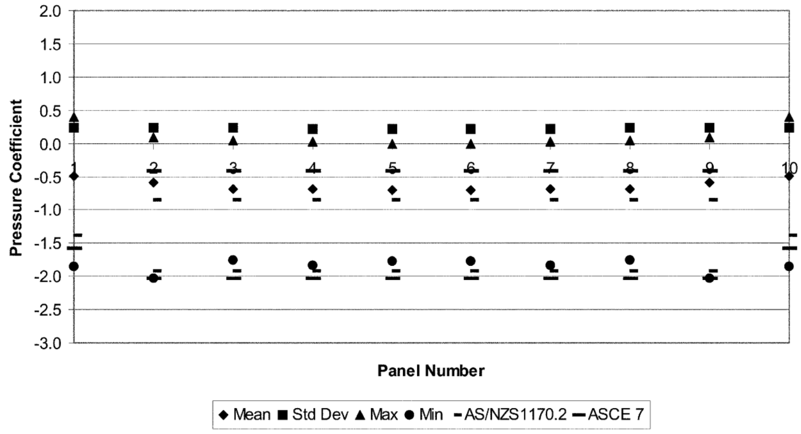

Fig. 4 Mean, standard deviation, maximum and minimum pressure coefficients on building configuration 1, $\theta = 90^o$ and effective peak pressure coefficients from AS/NZS 1170.2 and ASCE 7, $\theta = 90^o$

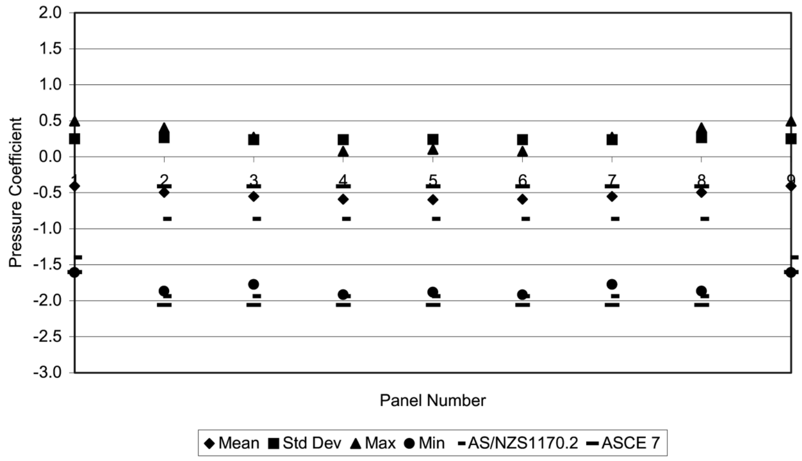

Fig. 5 Mean, standard deviation, maximum and minimum pressure coefficients on building configuration 2, $\theta = 90^o$ and effective peak pressure coefficients from AS/NZS 1170.2 and ASCE 7, $\theta = 90^o$

and 15 m of building configurations 1 and 2 respectively, in open approach terrain.

Fig. 2 shows that for building configuration 1, panel 1 on the windward wall and panels 2 to 4 on the windward roof slope are subjected to mean positive pressures whilst panels 6 to 9 on the leeward roof slope and panel 10 on the leeward wall experience large mean negative pressure coefficients. Furthermore, as described by Ginger and Holmes (2003), both AS/NZS 1170.2 and ASCE 7 are shown to underestimate the peak panel loads near the gable end on the leeward roof and wall of such buildings. Fig. 3, for building configuration 2, identifies larger discrepancies in pressure coefficients specified in AS/NZS 1170.2 and ASCE 7, with wind tunnel data. AS/NZS 1170.2 does not specify positive design pressures on the windward quarter of the roof. Figs. 4 and 5 show that flow separation and formation of the separation bubble at the gable-end generates large suction pressure coefficients on the roof and the sidewalls of building configurations 1 and 2.

6. Wind load effects for structural design

Fig. 6 shows the frame of building configuration 1 which is pinned at the apex and at the base (on 7.5 m high walls), as is typical of a 3-pin structural system used in such high roof pitch buildings. Fig. 7 shows the frame of building configuration 2, which is pinned at the base of the frame (on ground). The knee bending moments (M_{K1}, M_{K2} and M_{K3}, M_{K4}) and center rafter bending moments (M_{C1}, M_{C2} and M_{C3}) and horizontal reactions (R_{H1}, and R_{H2}) at the base of the frames are analysed here. The influence coefficients for windward and leeward knee bending moments, M_{K1} and M_{K2}, windward and leeward center rafter bending moments M_{C1} and M_{C2}, and horizontal reaction R_{H1} on the frame of building configuration 1 are listed in Table 2(a). The influence coefficients for windward and leeward knee

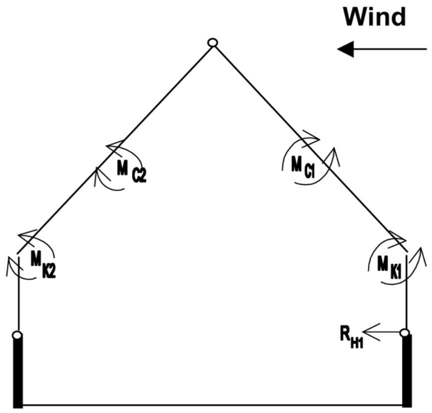

Fig. 6 Frame system of building configuration 1, attached to 7.5 m high walls showing selected load effects. Pin-joints at the apex and at the base of the frame-wall connections

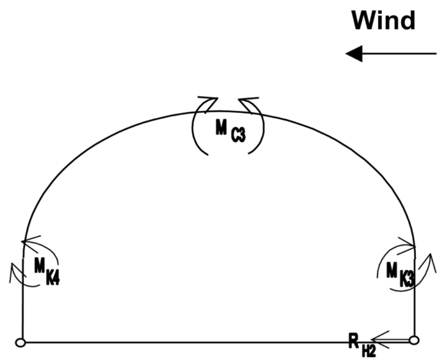

Fig. 7 Frame system of building configuration 2, showing selected load effects. Pin-joints at the base of the frame-ground connections

Table 2(a) Influence coefficients, building configuration 1

Load Effect	Panel									
	1	2	3	4	5	6	7	8	9	10
M_{K1} (kNm/kN)	3.10	3.02	1.95	0.89	-0.18	-4.48	-3.41	-2.35	-1.28	-0.65
M_{K2} (kNm/kN)	-0.65	-1.28	-2.35	-3.41	-4.48	-0.18	0.89	1.95	3.02	3.10
M_{C1} (kNm/kN)	1.55	3.04	5.55	5.02	1.44	-2.24	-1.71	-1.17	-0.64	-0.33
M_{C2} (kNm/kN)	-0.33	-0.64	-1.17	-1.71	-2.24	1.44	5.02	5.55	3.04	1.55
R_{H1} (kN/kN)	-0.91	-0.4	-0.26	-0.12	0.02	0.60	0.45	0.31	0.17	0.09

(b) Influence coefficients, building configuration 2

Load Effect	Panel								
	1	2	3	4	5	6	7	8	9
M_{K3} (kNm/kN)	3.40	5.28	2.77	0.32	-2.04	-3.62	-3.92	-3.44	-1.60
M_{K4} (kNm/kN)	-1.60	-3.44	-3.92	-3.62	-2.04	0.32	2.77	5.28	3.40
M_{C3} (kNm/kN)	-0.69	-1.09	-0.49	1.10	3.42	1.10	-0.49	-1.09	-0.69
R_{H2} (kN/kN)	-0.84	-0.53	-0.28	-0.03	0.00	0.36	0.39	0.34	0.16

Table 3(a) Wind load effects on frame near the gable-end, building configuration 1

Load effect coefficient	Covariance integration method, $\theta = 45^o$		AS/NZS 1170.2	ASCE 7
	Mean	Peak	$\theta = 0^o$	$\theta = 0^o$
CM_{K1}	0.067	0.104	0.105	0.099
CM_{K2}	-0.045	-0.080	-0.089	-0.079
CM_{C1}	0.042	0.091	0.091	0.080
CM_{C2}	-0.078	-0.109	-0.109	-0.102
CR_{H1}	-0.737	-1.247	-1.295	-1.257

(b) Wind load effects on frame near the gable-end, building configuration 2

Load effect coefficient	Covariance integration method, $\theta = 45^o$		AS/NZS 1170.2	ASCE 7
	Mean	Peak	$\theta = 0^o$	$\theta = 0^o$
CM_{K3}	0.080	0.173	0.195	0.231
CM_{K4}	-0.037	-0.096	-0.032	-0.073
CM_{C3}	-0.017	-0.053	-0.069	-0.076
CR_{H2}	-0.412	-0.998	-1.113	-1.313

bending moments, M_{K3} and M_{K4}, center rafter bending moment M_{C3} and horizontal reaction R_{H2} on the frame of building configuration 2 are listed in Table 2(b).

The bending moments and horizontal reactions are non-dimensionalised as, $C_M = M/[(1/2)\rho \bar{U}_h^2 d^2 w]$, and $C_R = R/\{(1/2)\rho \bar{U}_h^2 h_f w\}$ respectively, where d is the span of the building, w is the width of the tributary area and h_f is the height of the frame. Table 3(a) gives mean and peak positive and negative knee and center rafter bending moment coefficients, and the mean and peak horizontal reaction coefficient for building configuration 1, whilst Table 3(b) gives mean and peak positive and negative knee bending moment coefficients, mean and peak center rafter bending moment coefficient and the mean and peak horizontal reaction coefficients for building configuration 2, for $\theta = 45^o$. These peak values derived by the “covariance integration” method (Holmes and Best 1981), are compared with those calculated from AS/NZS 1170.2 (2002), ASCE 7 (2002). As detailed in (Ginger and Holmes 2003), whilst ASCE 7 slightly underestimates some design load effects on frames near the gable-end of long, planar roof buildings (i.e., building configuration 1), AS/NZS 1170.2 gives satisfactory load effects. However, design load effects determined from both AS/NZS 1170.2 and ASCE 7 for building configuration 2 compare less favorably against the covariance integration results, with the leeward knee bending moment significantly underestimated by AS/NZS 1170.2.

6.1. Eigenvector modes and eigenvalues

The fluctuating pressures on a tributary area can be presented as a series of eigenvector modes, as detailed in Section 3.1. Each eigenvector mode describes a loading mechanism and eigenvalue gives the proportion of pressure energy contributed by the mode. The first three eigenvector mode-shapes and the eigenvalues λ_1, λ_2, and λ_3 as a percentage of the sum of eigenvalues, λ_T for $\theta = 45^o$ and 90^o on building configurations 1, and 2 are given in Figs. 8 and 9, and Figs. 10 and 11, respectively.

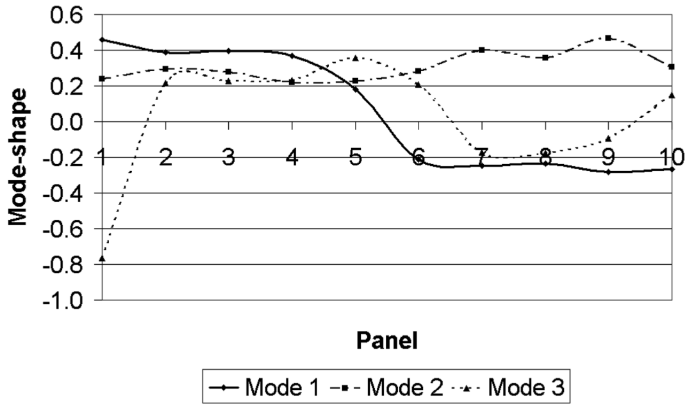

Fig. 8 Fluctuating wind load mode-shapes, building configuration 1, $\theta = 45^{\circ}$ $\lambda_1/\lambda_T = 0.38$, $\lambda_2/\lambda_T = 0.22$, $\lambda_3/\lambda_T = 0.12$

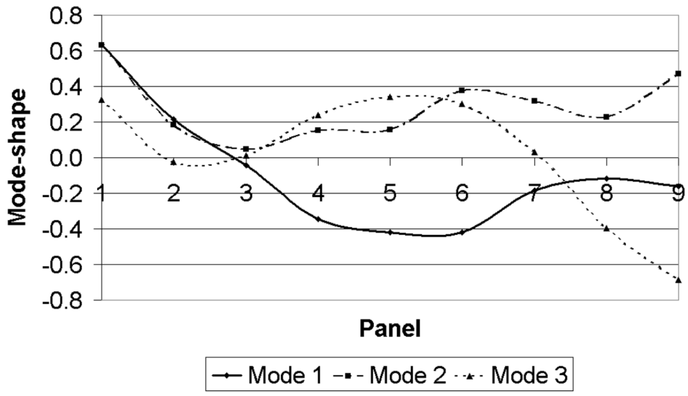

Fig. 9 Fluctuating wind load mode-shapes, building configuration 2, $\theta = 45^{\circ}$ $\lambda_1/\lambda_T = 0.41$, $\lambda_2/\lambda_T = 0.23$, $\lambda_3/\lambda_T = 0.14$

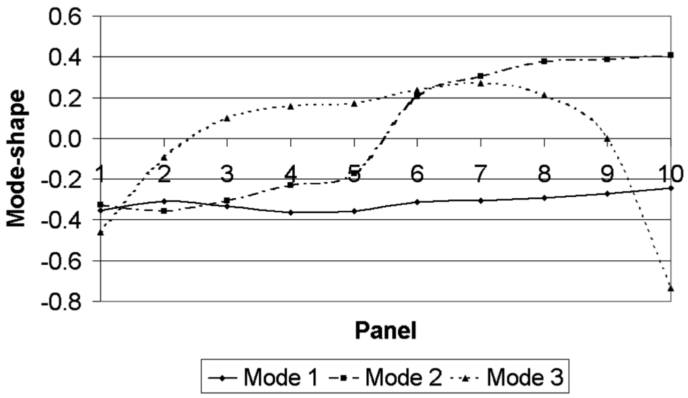

Fig. 10 Fluctuating wind load mode-shapes, building configuration 1, $\theta = 90^{\circ}$ $\lambda_1/\lambda_T = 0.38$, $\lambda_2/\lambda_T = 0.20$, $\lambda_3/\lambda_T = 0.13$

These figures indicate that the first mode contributes about 40% to the total fluctuating pressure energy, and has a mode-shape that generally follows the mean pressure distribution. Previous studies

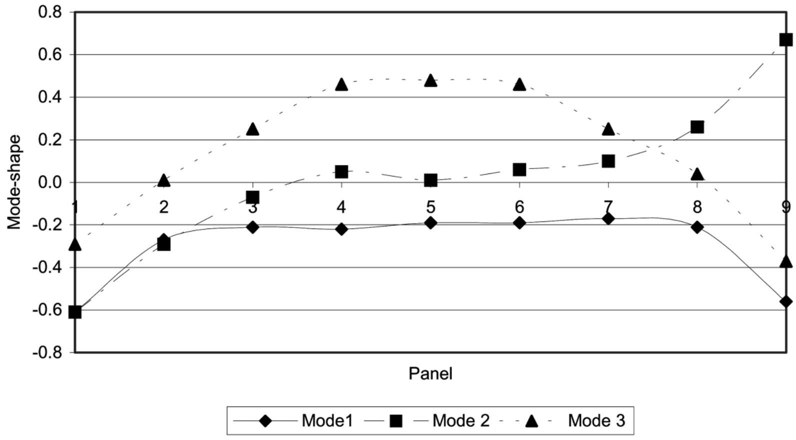

Fig. 11 Fluctuating wind load mode-shapes, building configuration 2, $\theta = 90^{\circ}$ $\lambda_1/\lambda_T = 0.37$, $\lambda_2/\lambda_T = 0.23$, $\lambda_3/\lambda_T = 0.16$

Table 4(a) Variance of load effects and first eigenvector contributions, and coefficient of determination between first mode shape and influence line, building configuration 1, $\theta = 45^{\circ}$

Coefficient			Percent contribution to fluctuating load effect from first mode	R^2
Load Effect	Variance	$\alpha_1^2\,\lambda_1$		
CM_{K1}	7.60E-5	6.74E-5	89%	0.76
CM_{K2}	6.71E-5	5.86E-5	87%	0.59
CM_{C1}	1.01E-4	9.19E-5	91%	0.75
CM_{C2}	8.51E-5	5.69E-5	69%	0.65
CR_{H1}	1.18E-2	1.05E-2	89%	0.70

(b) Variance of load effects and first eigenvector contributions, and coefficient of determination between first mode shape and influence line, building configuration 2, $\theta = 45^{\circ}$

Coefficient			Percent contribution to fluctuating load effect from first mode	R^2
Load Effect	Variance	$\alpha_1^2\,\lambda_1$		
CM_{K3}	3.17E-4	2.74E-4	87%	0.51
CM_{K4}	1.36E-4	9.92E-6	7.3%	0.03
CM_{C3}	5.41E-5	3.92E-5	72%	0.38
CR_{H2}	1.15E-2	9.72E-3	85%	0.68

by Holmes and Best (1981), Holmes (1988) and Ginger (2003) have described eigenvectors of pressure fluctuations on tributaries and their eigenvalue contributions to the fluctuating pressures.

Tables 4(a) and 4(b) present the variance (in coefficient form) of the knee bending moment, center rafter bending moment and horizontal reaction coefficients on building configurations 1, and 2 respectively, for $\theta = 45^{\circ}$, derived from the "covariance integration" method, and the contribution to these fluctuating load effects from the first eigenvector mode. Furthermore, the coefficient of determination R^2 between the first mode shape and the influence lines (which is a measure of the

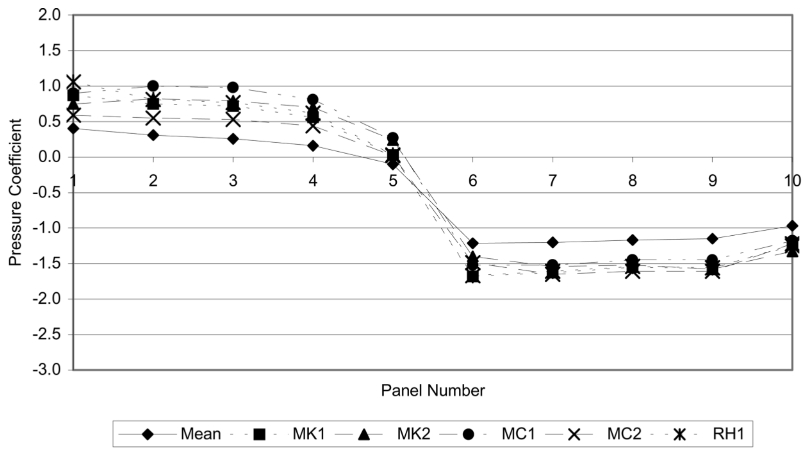

Fig. 12 Mean and effective static pressure coefficient distribution on frame for M_{K1}, M_{K2}, M_{C1}, M_{C2} and R_{H1} on building configuration 1, $\theta = 45^{o}$

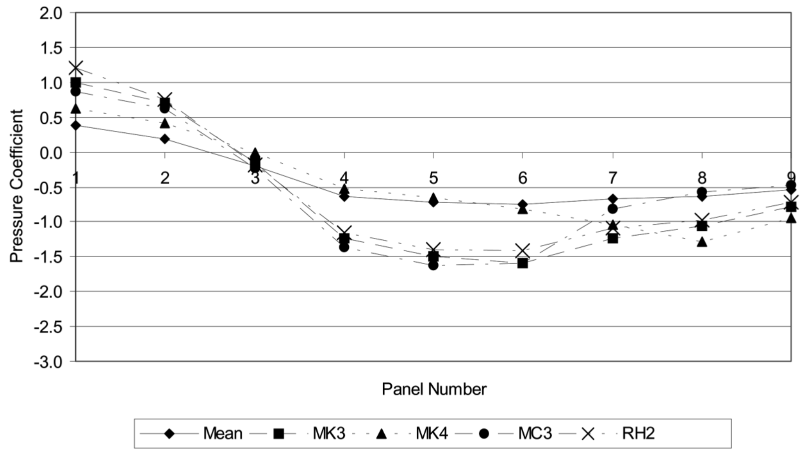

Fig. 13 Mean, and effective static pressure coefficient distribution on frame for M_{K3}, M_{K4}, M_{C3} and R_{H2} on building configuration 2, $\theta = 45^{o}$

similarity of the mode shape and influence line, where R^2 is a maximum value of 1.0 for matching shapes) are also listed in Tables 4(a) and 4(b). Tables 4(a) and 4(b) show that $R^2 > 0.50$ and the first mode contributes about 90% to the fluctuations of the load effects which have influence line shapes that closely match the first mode shape (i.e., M_{K1}, M_{K2}, M_{C1}, R_{H1}, M_{K3}, R_{H2}), whilst the contribution decreases to less than 10% and $R^2 < 0.05$, when the influence line does not match the first mode shape (i.e., M_{K4}).

The effective static pressure distributions generating the peak values of M_{K1}, M_{K2}, M_{C1}, M_{C2} and R_{H1}, on building configuration 1, for $\theta = 45^{o}$ derived from the LRC method are presented in Fig. 12. Each of these distributions which are enveloped between the maximum and minimum pressure coefficients given in Fig. 2, are generally similar in shape to the mean pressure distribution, reflecting the relatively large contribution to these load effect fluctuations from the first mode. The effective static pressure distributions for the peak values of M_{K3}, M_{K4}, M_{C3} and R_{H2}, on building configuration 2, for $\theta = 45^o$ derived from the LRC method are presented in Fig. 13. In this case, although the effective static pressure distributions for M_{K3}, M_{C3} and R_{H2}, closely follow the mean pressure, the effective static pressure distribution for M_{K4} does not, as the first mode contributes less than 10% to its fluctuations.

7. Conclusions

Wind tunnel model studies were carried out to determine the wind loading characteristics on frame tributaries near the gable-end of two buildings with steep roofs; a 35^o planar roof - configuration 1, and a curved roof - configuration 2. Fluctuating pressures acting on these tributaries were analysed, and wind load effects for structural design (i.e., knee bending moments, center rafter bending moments and horizontal support reactions at the base of the fames) studied.

Background pressure fluctuations on frame tributaries near the gable-end were presented as a series of uncorrelated modes given by the eigenvectors of the force covariance matrix. Analysis of eigenvalues show that the dominant first mode contributes around 40% to the fluctuating pressures, and that the mode-shapes generally follow the mean pressure distributions on building configurations 1 and 2.

The contribution from each eigenvector mode to the fluctuating component of the load effect of interest is dependent on the similarity in the shapes of the influence line for the load effect and the eigenvector mode-shape. The first mode contributes more than 68% to the fluctuating windward knee bending moment and horizontal reaction on the frame of building configurations 1 and 2, the windward and leeward center-rafter bending moments of building configuration 1, and the center rafter bending moment at the apex of building configuration 2. In these cases, the effective static pressure distribution obtained from the "load response correlation" (LRC) method closely follows the mean pressure distribution on the tributary, and quasi-static method would provide a satisfactory estimate of peak load effects.

References

American Society of Civil Engineers (2002), *Minimum Design Loads for Buildings and Other Structures*, ASCE 7-02.

AS/NZS 1170.2 Structural design actions - Part 2: Wind actions (2002).

Ginger, J.D. and Holmes, J.D. (2001), "Wind loads on long, low-rise buildings", *Proc. 5th Asia Pacific Conf. on Wind Engineering*, Kyoto, Japan, 529-532.

Ginger, J.D. and Holmes, J.D. (2003), "Effect of building length on wind loads on low-rise buildings with a steep roof pitch", *J. Wind Eng. Ind. Aerody.*, **91**, 1377-1400.

Ginger, J.D. (2003), "Fluctuating wind pressures across gable-end buildings", *Preprints 11th Int. Conf. on Wind Engineering, Vol. 1,* Lubbock, Texas, USA, 1214-1220.

Holmes, J.D. and Best, R.J. (1981), "An approach to the determination of wind load effects on low-rise buildings", *J. Wind Eng. Ind. Aerody.*, **7**, 273-287.

Holmes, J.D. (1988), "Analysis and synthesis of pressure fluctuations on bluff bodies using eigenvectors", *International Colloquium on Bluff Body Aerodynamics and its Applications*, Kyoto, Japan, 291-302.

Holmes, J.D. (1992), "Optimized peak load distributions", *J. Wind Eng. Ind. Aerody.*, **41-44**, 267-276.

Holmes, J.D. (2002), "Effective static load distributions in wind engineering", *J. Wind Eng. Ind. Aerody.*, **90**, 91-

109.
Kasperski, M. and Niemann, H.J. (1989), “Identification of critical load distributions for wind loading”, *5th Int. Conf. on Structural Safety and Reliability*, San Francisco, USA.

MM